

# Recent progress in high-efficiency silicon heterojunction solar cells at EPFL and CSEM

*A. Descoeurdes<sup>1,2</sup>, C. Allebé<sup>2</sup>, N. Badel<sup>1,2</sup>, L. Barraud<sup>1,2</sup>, F. Debrot<sup>2</sup>, B. Demareux<sup>1</sup>, A. Faes<sup>2</sup>, J. Geissbühler<sup>1</sup>, N. Holm<sup>1</sup>, Z. C. Holman<sup>1</sup>, J. Holovsky<sup>1</sup>, S. Martin de Nicolas<sup>1</sup>, S. Nicolay<sup>2</sup>, B. Paviet-Salomon<sup>1</sup>, L. Sansonnens<sup>2</sup>, J. Seif<sup>1</sup>, A. Tomasi<sup>1</sup>, M. Despeisse<sup>2</sup>, S. De Wolf<sup>1</sup>, and C. Ballif<sup>1,2</sup>*

1. Ecole Polytechnique Fédérale de Lausanne (EPFL), Institute of Microengineering (IMT), Photovoltaics and Thin-Film Electronics Laboratory, CH-2000 Neuchâtel, SWITZERLAND

2. Centre Suisse d'Electronique et de Microtechnique (CSEM), PV-center, CH-2002 Neuchâtel, SWITZERLAND

## ABSTRACT

Improvements in the efficiency of silicon heterojunction solar cells are obtained by working on surface passivation, front- and back-side optical properties, and metallization. The highest aperture-area certified efficiencies obtained on 4 cm<sup>2</sup> screen-printed cells are 22.14% and 21.38% on *n*- and *p*-type FZ wafers, respectively, whereas efficiencies over 21% are achieved with three different types of PECVD systems.

## 1. INTRODUCTION

For any high-efficiency crystalline silicon (c-Si) solar cell, high-quality surface passivation is of extreme importance. Silicon heterojunction (SHJ) solar cells are fabricated by depositing thin hydrogenated amorphous silicon (a-Si:H) layers on c-Si wafers for this purpose<sup>[1]</sup>. This design enables energy conversion efficiencies well above 20% (up to 24.7% currently<sup>[2]</sup>) at a reasonable cost, and is being pursued by an increasing number of groups. The key feature of SHJ cells is that the metal contacts, which are highly recombination active in traditional diffused-junction cells, are moved away from the absorber by insertion of the wider bandgap a-Si:H layers. This explains the record open-circuit voltages ( $V_{oc}$ )

typically associated with this device design, without the need for expensive patterning techniques. In this contribution, we will review the recent progress we made in this technology.

## 2. SHJ SOLAR CELL FABRICATION

The typical structure of a SHJ solar cell is drawn in figure 1. Unless otherwise stated, *n*-doped float-zone (FZ) textured wafers were used as substrates. Intrinsic and doped a-Si:H layers were deposited by plasma-enhanced chemical vapour deposition (PECVD) in different reactors: a modified industrial KAI-M (40 MHz, 50 x 60 cm<sup>2</sup> electrode size), an Octopus I (13 & 40 MHz, 15 x 16 cm<sup>2</sup>) and a new Octopus II (13 & 40 MHz, 40 x 50 cm<sup>2</sup>) cluster tool (by INDEOtec). Transparent conductive oxide (TCO), typically indium tin oxide (ITO), was then deposited by DC magnetron sputtering, and a silver back reflector as well. A front grid was screen-printed with a low temperature silver paste. Note that all of these fabrication steps<sup>[3]</sup> are compatible with cell production at an industrial scale.

## 3. RESULTS

### 3.1 Amorphous silicon passivation layers

Intrinsic a-Si:H films are already known for a few decades to yield good c-Si surface

passivation. From deposition perspective, we found that highly-depleted silane ( $\text{SiH}_4$ ) plasmas (i.e. regimes close to the amorphous-to-crystalline transition) yield the best electronic properties<sup>[4]</sup>. A critical condition for the latter is the purveyance of an atomically sharp a-Si:H/c-Si interface, however<sup>[5]</sup>. To come closer to the transition without risking detrimental epitaxial growth,  $\text{H}_2$  plasma treatments during a-Si:H growth via brief deposition interruptions were proven to be very effective<sup>[6]</sup>.

To fabricate emitter and back surface fields, doped a-Si:H must be deposited on the passivating intrinsic a-Si:H layers with sufficient care, else Fermi-level induced defect generation in the passivation layers underneath may occur<sup>[7]</sup>. Subsequently, TCO layers need to be deposited for contact formation. Such depositions may equally detrimentally affect the surface passivation of the device, which is at least partially caused by plasma luminescence during TCO sputtering<sup>[8]</sup>.

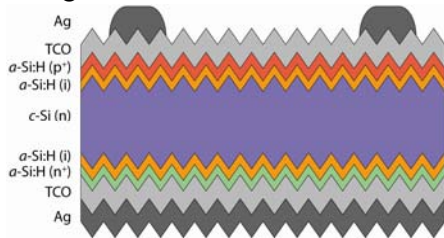


**Fig. 1** Typical structure of a SHJ solar cell<sup>[11]</sup>.

### 3.2 Front-side transparency

Reduction of parasitic light absorption occurring in the front a-Si:H and TCO layers is also required to reach high efficiencies, since a loss over  $2 \text{ mA/cm}^2$  can be attributed to this phenomenon<sup>[9]</sup>. This can be achieved for example by implementing wider bandgap materials such as amorphous silicon oxide<sup>[10]</sup>, or microcrystalline silicon<sup>[11]</sup> instead of a-Si:H. The replacement of the front ITO layer by a higher mobility TCO, such as hydrogen-doped indium oxide

(IO:H) for example<sup>[12]</sup>, enables also an improved front-side transparency. Figure 2a shows the absorbance of 110 nm IO:H and ITO films on glass. The films have approximately the same sheet resistance, but the electron density is three times lower and the mobility is three times larger in the IO:H film. Free carrier absorption in the IO:H film is thus approximately nine times lower than that in the ITO film. SHJ solar cells with IO:H as the front TCO material exhibit higher IR response than those with ITO. Figure 2b displays the external quantum efficiency (EQE) and total absorbance (1-reflectance) of solar cells with IO:H and ITO front electrodes like those in Fig. 2a. The spectra nearly overlap at short wavelengths, but IR parasitic absorption (shaded area) is reduced in the cell with IO:H. Consequently, although the TCO layers have the same sheet resistance, the active-area short-circuit current density ( $J_{sc}$ ) is  $1.0 \text{ mA/cm}^2$  larger for the cell with IO:H.

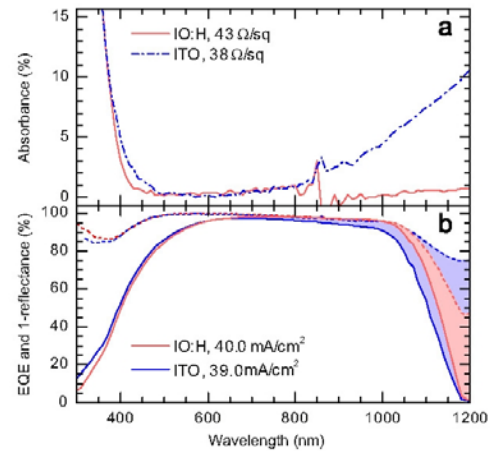


**Fig. 2** (a) Absorbance spectra of IO:H and ITO films on glass. (b) External quantum efficiency (solid) and 1-reflectance (dashed) spectra of SHJ solar cells with IO:H and ITO front contacts<sup>[12]</sup>.

### 3.3 Back-side reflectivity

Infrared parasitic absorption in SHJ solar cells arises from free-carrier absorption in

both the front and rear TCO layers, as well as plasmonic absorption in the rear metal electrode<sup>[13]</sup>. One method to mitigate the loss in the metal electrode is to require the rear TCO layer to play an optical as well as electrical role by making it thick and very transparent<sup>[13]</sup>. An alternative approach is to make the rear TCO very thin so that it serves only an electrical contact function, and to add another layer specifically to suppress plasmon excitation in the metal electrode.

For this purpose, we have fabricated rear reflectors with low-refractive-index magnesium fluoride ( $\text{MgF}_2$ ) as the dielectric, and with local electrical contacts through the  $\text{MgF}_2$  layer<sup>[14]</sup>. These  $\text{MgF}_2$ /metal reflectors are introduced into cells in place of the usual TCO/metal reflector. An  $\text{MgF}_2$ /Ag reflector yields an average rear internal reflectance of greater than 99.5% and an infrared internal quantum efficiency that exceeds that of the world-record UNSW PERL cell (figure 3). An  $\text{MgF}_2$ /Al reflector performs nearly as well.

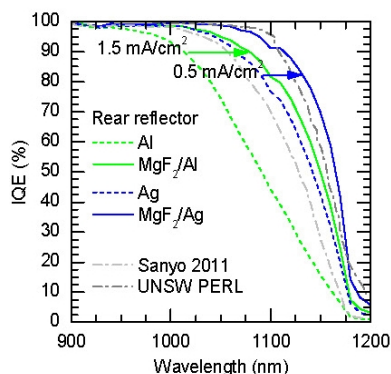


**Fig. 3** Internal quantum efficiency of SHJ solar cells with and without  $\text{MgF}_2$  layers, and with aluminum or silver rear electrodes<sup>[14]</sup>.

### 3.4 Advanced front-side metallization

To improve the front-side metallization of SHJ solar cells, we have investigated electrodeposition of copper<sup>[15]</sup>. Replacing the silver-paste by high-conductivity

electrodeposited copper allows simultaneously to reduce the finger-width and to realize a cost reduction. Moreover, shadow losses due to paste spreading are avoided with electrodeposition. Fingers below  $10\ \mu\text{m}$  with a 1:1 aspect ratio were obtained by using photolithography as the patterning technique (figure 4). To overcome the low-adhesion of copper on the front TCO, a  $1\ \mu\text{m}$  thick nickel layer is created before the copper electrodeposition. The electrical resistivity is found to be close from the bulk value of copper.

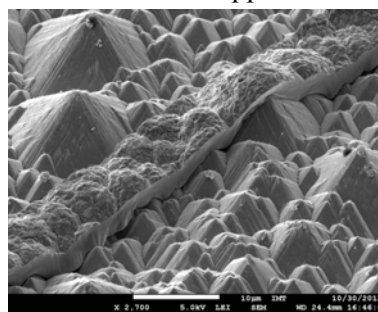


**Fig. 4** SEM picture of a  $10\ \mu\text{m}$  Ni/Cu plated finger on a textured wafer covered with TCO<sup>[15]</sup>.

### 3.5 Influence of wafer doping type

We have also compared the use of  $n$ -type versus  $p$ -type c-Si substrates<sup>[3]</sup>. The most notable difference is found in the fill factor (FF) of these devices. The lower FF value for  $p$ -type wafers is fundamentally linked to the electronic properties of the c-Si surface dangling bond. The asymmetry in interface defect capture cross sections for holes and electrons results indeed in reduced minority carrier lifetime at low injection for the  $p$ -type case (figure 5).

By using high-quality passivation layers, however, these losses can be minimized. High  $V_{\text{oc}}$ s were obtained on both types of float zone wafers: up to 735 mV on  $n$ - and 726 mV on  $p$ -type. The highest aperture-area certified efficiencies obtained on  $4\ \text{cm}^2$  cells (with screen-printed front metallization)

were 22.14% and 21.38% on  $n$ - and  $p$ -type FZ wafers, respectively, proving that heterojunction schemes can perform almost as well on high-quality  $p$ -type as on  $n$ -type wafers<sup>[3]</sup>. To our knowledge, this is the highest efficiency ever reported for a full SHJ solar cell on a  $p$ -type wafer, and the highest  $V_{oc}$  on any  $p$ -type crystalline silicon device with reasonable FF.

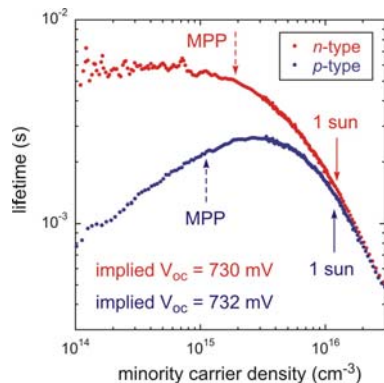


**Fig. 5** Minority carrier effective lifetimes of solar cell precursors on  $n$ - and  $p$ -type FZ wafers ( $4 \Omega \cdot \text{cm}$ )<sup>[3]</sup>.

Finally, we give in Table I the parameters of the best cells produced in the different PECVD reactors. Noticeably, our good control of plasma processes allow reaching high efficiencies when using state-of-the-art equipments. For example, the 22.4% cell made in the new Octopus II reactor was obtained after only a couple of months of layer development.

**Table I** Best  $4 \text{ cm}^2$  cells produced in the different PECVD reactors ( $n$ -doped  $c$ -Si)

	KAI	Octopus I	Octopus II
$V_{oc}$ [mV]	727	723	727
$J_{sc}$ [mA/cm <sup>2</sup> ]	38.9	37.5	39.2
FF [%]	78.4	78.7	78.6
Eff. [%]	22.1*	21.3	22.4

\* certified by the Fraunhofer ISE Callab<sup>[3]</sup>

#### 4. CONCLUSIONS

Continuous improvement in SHJ solar cells were obtained with the different approaches discussed in this paper. These results give further evidence how heterojunction technology offers an interesting route towards high-efficiency industrial solar cells.

#### 5. ACKNOWLEDGMENTS

This work was supported by the Axpo Naturstrom Fonds, by the European Commission FP7 project 20plus, by the Swiss Commission for Technology and Innovation, by Roth & Rau Research, and by the EuroTech Universities Alliance.

#### REFERENCES

- [1] S. De Wolf et al., *Green*, **2**, 7 (2012).
- [2] M. Taguchi et al., *39<sup>th</sup> IEEE PVSC*, Tampa, USA (2013).
- [3] A. Descoeurdes et al., *IEEE J. Photovoltaics*, **3**, 83 (2013).
- [4] A. Descoeurdes et al., *Appl. Phys. Lett.*, **97**, 183505 (2010).
- [5] S. De Wolf et al., *Appl. Phys. Lett.*, **90**, 042111 (2007).
- [6] A. Descoeurdes et al., *Appl. Phys. Lett.*, **99**, 123506 (2011).
- [7] S. De Wolf et al., *J. Appl. Phys.*, **105**, 103707 (2009).
- [8] B. Demarex et al., *Appl. Phys. Lett.*, **101**, 171604 (2012).
- [9] Z. C. Holman et al., *IEEE J. Photovoltaics*, **2**, 7 (2012).
- [10] J. Seif et al., to be published.
- [11] J. Seif et al., *ICANS 25*, Toronto, Canada (2013).
- [12] L. Barraud et al., *Sol. Energy Mater. Solar Cells*, **115**, 151 (2013).
- [13] Z. C. Holman et al., *J. Appl. Phys.*, **113**, 013107 (2013).
- [14] Z. C. Holman et al., *IEEE J. Photovoltaics*, accepted for publication.
- [15] J. Geissbühler et al., to be published.